separations

MDPI

Article

Efficient and Rapid Removal of Cationic Methylene Blue from Aqueous Solution by Alkali-Treated Bamboo Powders as Biosorbents

Qin Wang [1], Yaohui Xu [1,2,3,*], Jinqiang Yu [1], Runhong Xia [1], Zhiyun Jiang [1], Yuan Zhang [1] and Fangyu Xiong [4,*]

[1] Laboratory for Functional Materials, School of New Energy Materials and Chemistry, Leshan Normal University, Leshan 614000, China; wq306115@lsnu.edu.cn (Q.W.); yujq20220901@163.com (J.Y.); xiar200424@163.com (R.X.); jzy123456kij@163.com (Z.J.); zy112504@163.com (Y.Z.)
[2] Sichuan Province Key Lab for Bamboo Pest Control and Resource Development, Leshan 614000, China
[3] Leshan West Silicon Materials Photovoltaic and New Energy Industry Technology Research Institute, Leshan 614000, China
[4] National Engineering Research Center for Magnesium Alloys, College of Materials Science and Engineering, Chongqing University, Chongqing 400044, China
* Correspondence: xyh1986@lsnu.edu.cn (Y.X.); xfy@cqu.edu.cn (F.X.); Tel.: +86-0833-2270785 (Y.X.); +86-023-65127881 (F.X.)

Abstract

To develop low-cost and renewable materials for treating dye wastewater, an efficient biosorbent was prepared from *Bambusa emeiensis* bamboo powders (BPs) via a simple alkali pretreatment. Systematic investigation revealed that NaOH concentration was critical for enhancing adsorption performance. Under optimal conditions (NaOH $\geq$ 0.2 mol/L, dosage = 10.0 g/L), the BPs achieved over 96% removal of cationic Methylene Blue (MB, 20 mg/L) within 20 min, demonstrating rapid kinetics. The adsorption process followed the Langmuir isotherm model with a maximum adsorption capacity of 4.1 mg/g without adjusting the pH of the solution and complied with the pseudo-second-order kinetic model. Thermodynamic analysis confirmed the spontaneous ($\Delta G < 0$) and exothermic ($\Delta H = -52.73$ kJ/mol) nature of the adsorption. Notably, the alkali-treated BPs exhibited a pronounced preference for the cationic dye, achieving a high removal rate of 96.5% for MB, in contrast to a much lower removal of 23.6% for the anionic dye AO7 under identical single-dye conditions, attributed to the enhanced surface negative charge after alkali treatment. Furthermore, the BPs maintained a high removal efficiency of 91.2% after eight adsorption-desorption cycles using 0.1 mol/L HCl as eluent, demonstrating excellent reusability. This study presents a feasible and sustainable strategy for designing regenerative bamboo-based biosorbents with rapid and preferential adsorption capabilities for cationic dye wastewater.

Keywords: bamboo powders; biosorbent; Methylene Blue; alkali treatment; adsorption; regeneration

Check for updates

Academic Editors: Kunlun Yang, Jian Mei, Feilong Zhang and Jingzhen Zhang

Received: 31 December 2025
Revised: 31 January 2026
Accepted: 4 February 2026
Published: 6 February 2026

Copyright: © 2026 by the authors. Licensee MDPI, Basel, Switzerland. This article is an open access article distributed under the terms and conditions of the Creative Commons Attribution (CC BY) license.

1. Introduction

The invention and extensive application of synthetic dyes represent a significant milestone in modern industrial development, having substantially enhanced product performance and aesthetics in textiles, printing, plastics and pharmaceuticals, while profoundly transforming modern lifestyles [1,2]. However, the subsequent discharge of large volumes of dye-containing wastewater has raised serious environmental concerns. Untreated effluent causes aesthetic water pollution, impedes light penetration and introduces dyes

with mutagenic and potential carcinogenic risks. These contaminants can bioaccumulate through the food chain, ultimately endangering human health by inducing symptoms ranging from eye injuries and digestive disorders to tissue necrosis [3,4]. Consequently, developing efficient dye removal technologies is of urgent importance for protecting aquatic environments and public health.

Among the various methods for wastewater treatment [5–7], adsorption is regarded as one of the most promising technologies due to its operational simplicity, high efficiency, and process flexibility [8–10]. The performance of adsorbents is a critical factor in this context [11,12]. Although activated carbon exhibits excellent adsorption capacity, its limitations include high raw material costs, energy-intensive production, potential secondary pollution and excessive consumption of resources such as timber, which conflicts with sustainable development principles [13]. Precisely because of these constraints, the search for alternative adsorbents with wide availability, low cost, and environmental friendliness has become a central driving force in current research [14]. This has led to a surge of interest in utilizing renewable biomass as raw materials for next-generation adsorbents.

Renewable biomass resources have garnered significant attention as promising, low-cost, and eco-friendly adsorbents, embodying the sustainable principle of "treating waste with waste" [15,16]. Extensive research has explored diverse biomass sources, such as agricultural wastes (e.g., fruit peels and seeds), lignocellulosic residues and other agro-industrial by-products, for dye removal. Table 1 summarizes representative studies, highlighting variations in pretreatment methods, target dyes, equilibrium time, and adsorption capacity. However, the quest for an ideal biomass adsorbent that combines high efficiency, simple processing, stability, and year-round availability continues.

Table 1. Summary of studies on dye removal using biomass-derived adsorbents. (q_{max}: maximum adsorption capacity).

Biomass Source	Pre-Treatment	Target Dye	Equilibrium Time	q_{max} (mg/g)
Activated carbon [17]	Derived from rice husk: 50 vol.% H_3PO_4, 500 °C, 2.5 h	Acid Blue	10 h	50
Activated carbon [18]	Supplied by BDH Laboratory Supplies, Poole, UK	Methyl Red	180 min	48.4
Sugarcane bagasse [18]	Concentrated H_3PO_4: 150 °C, 24 h (250–350 µm)	Methyl Red	180 min	11.0
Waste orange peel [19]	Cut into small pieces, dried in sunlight and crushed.	Congo Red; Procion Orange; Rhodamine B	90 min; 25 min; 20 min	22.4; 1.33; 3.23
Sugar cane dust [20]	Depithing, powdering and screening	Malachite Green; Rhodamine B	14 min	4.88; 4.26
Cupuassu shell [21]	oven at 70 °C for 8 h; Crushing and screening; ≤250 µm	Reactive Red 194; Direct Blue 53	8 h; 18 h	64.1; 37.5
Caulerpa lentillifera [22]	Washed and dried at 80 °C for 12 h	Astrazon Blue; Astrazon Red; Methylene Blue	10 min; 30 min; 30 min	38.9; 47.6 417
Canola hull [23]	Washing, dried, crushing and screening at ≤125 µm	Basic Blue 41; Basic Red 46; Basic Violet 16	~20 min	67.6 49.0 25.0

Table 1. *Cont.*

Biomass Source	Pre-Treatment	Target Dye	Equilibrium Time	q_{max} (mg/g)
Tamarind Fruit Shell [24]	Washing, dried, crushing and screening at ≤177 μm	Methylene Blue	~45 min	1.72
Mangifera indica (mango) seeds [25]	Washing, dried, crushing and screening at ≤106 μm	Victazol Orange 3R	5 h	71.6
Sawdust [26]	Modified by Sodium dodecyl sulfate solution (10 g/L), 12 h at room temperature	Methylene Blue	60 min	130.7
Peanut hull [27]	Washing, dried, crushing and screening at 80–100 mesh	Amaranth; Sunset Yellow; Fast Green FCF	~25 h	14.9 14.0 15.6
Phragmites australis [28]	NaOH solution (1.0 mol/L), epichlorohydrin; refluxing: isopropyl alcohol, Na_2SO_3, 4 h; refluxing: H_2SO_4 (0.5 mol/L), 2 h.	Methylene Blue	90 min	46.8
Aqai palm stalk [29]	HCl (3 mol/L); ≤250 μm	Procion Blue MX–R	8 h	71.65

In this context, bamboo, often hailed as "the second forest" due to its remarkable growth rate, high yield, and excellent renewability, emerges as a superior candidate. Beyond its rapid growth and renewability, bamboo possesses an intrinsic, hierarchical porous structure composed of natural micro- and nano-fibrils, along with an abundance of surface functional groups (e.g., hydroxyl, carboxyl), which provide a solid physicochemical foundation for adsorption applications [30]. Its high mechanical strength also promises good durability in water treatment systems.

Despite this inherent potential, many conventional methods to transform bamboo into efficient adsorbents involve energy-intensive procedures such as high-temperature carbonization or complex chemical modifications, which can offset their economic and environmental benefits. To address this gap, this study innovatively proposes a streamlined strategy using *Bambusa emeiensis*, a widely available species in the study region. We demonstrate that a simple, controlled-concentration alkali (NaOH) pretreatment at room temperature is sufficient to activate the bamboo powders (BPs) by effectively removing soluble organics and enhancing surface negativity. This approach aims to unlock the innate adsorption capability of bamboo with minimal processing, targeting the efficient removal of cationic dyes like Methylene Blue (MB).

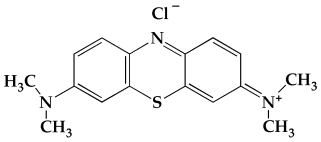
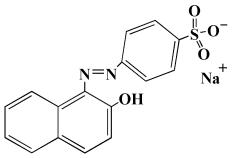
Furthermore, to elucidate the role of electrostatic interactions in the adsorption mechanism, the anionic dye Acid Orange 7 (AO7) was employed as a comparative adsorbate, highlighting the enhanced adsorption affinity for cationic dyes arising from electrostatic interactions. Consequently, this work aims to provide comprehensive evidence and theoretical guidance for developing cost-effective and readily reusable bamboo-based adsorbents with enhanced affinity for cationic pollutants, thereby advancing the innovative application of bamboo resources in sustainable water treatment technologies.

2. Experimental Procedure

2.1. Starting Materials

The primary information for Methylene Blue (MB) and Acid Orange 7 (AO7) is presented in Table 2. Moreover, sodium hydroxide (NaOH, AR, 97%) and hydrochloric acid (HCl, AR, 36–38%) were purchased from Chengdu Kelong Chemical Co., Ltd. (Chengdu, China). Purified water was employed in the formulation of dye-simulated wastewater, as well as in the preparation of NaOH alkaline solution and HCl acid eluent.

Table 2. Primary information for MB and AO7 dyes.

Name	Types of Dyes	Manufacturers	Specification	Chemical Formula
Methylene Blue (MB)	Cationic dye	Bide Pharmatech Co., Ltd. (Shanghai, China)	98.0%	
Acid Orange 7 (AO7)	Anionic dye	Shanghai Maclin Biochemical Technology Co., Ltd. (Shanghai, China)	97.0%	

2.2. Pretreatment of Biosorbent BPs

A species of bamboo known as *Bambusa emeiensis* was utilized as the raw material, sourced from a nearby region in Leshan, China. The bamboo stems were stripped of leaves, dried, crushed into powder using a pulverizer, and finally sieved to the desired particle sizes (e.g., 60 mesh). The bamboo powders (BPs) obtained above were rinsed with running water to eliminate adherent dust and other unwanted particles. Subsequently, approximately 50.0 g of BPs were immersed in 1000 mL of NaOH aqueous solution at varying concentrations for a duration of 24 h. During this period, the initially colorless NaOH solution gradually turned brown, visually confirming the dissolution of organic components (e.g., hemicellulose, lignin, and likely polyphenolic compounds) from the biomass. This step aimed to remove residual soluble organic components, such as hemicellulose and lignin, from the BPs matrix. To minimize the potential interference from any dissolved organics (including phenolic compounds) and to neutralize the material, the treated BPs were thoroughly filtered and then rinsed copiously with purified water. The rinsing was continued until the rinse water became completely clear and its pH was stable at approximately neutral (pH ~7). This rigorous washing procedure was critical to obtain a well-cleaned adsorbent surface for the subsequent adsorption studies. The final biological material (BPs) was obtained after drying at 60 °C for 24 h and subsequently stored in a ziplock bag for future use.

2.3. Preparation of Dye Solution

The cationic dye MB was meticulously chosen as the primary target pollutant.

To contrast the adsorption behavior and demonstrate the dominant role of electrostatic interactions, the anionic dye AO7 was employed alongside MB as a comparative adsorbate. The MB and AO7 powders were analytically pure, were used without further purification. Aqueous solutions of MB and AO7 dyes at varying concentrations were prepared from a stock solution of 1.0 g/L through precise dilution techniques.

2.4. Batch Adsorption Experiments

Batch adsorption experiments were conducted using a HY–5A rotary shaker (Shanghai Lichen Instrument Technology Co., Ltd., Shanghai, China) at room temperature. In each experiment, 100 mL of dye aqueous solution with an initial concentration of 20 mg/L was treated with 1.0 g of BPs biosorbent. Following agitation under continuous stirring at a rate of 200 r/min, aliquots of the dye solution were promptly filtered through a 0.22 μm glass fiber syringe filter (Hunan BKMAM Holding Co., Ltd., Changde, China) to separate the adsorbent. The clear filtrate was then immediately analyzed for dye concentration using a U–3900 UV–visible spectrophotometer (Hitachi, Tokyo, Japan). To account for potential background interference from the biosorbent itself, a control experiment was conducted in which BPs were agitated in purified water under identical adsorption conditions. The filtrate exhibited negligible absorbance in the spectral range used for dye quantification (750–400 nm), confirming that the observed decrease in dye absorbance was attributable solely to adsorption. Similar measurements were performed under varying conditions including contact time, initial concentration, temperature and pH levels. Temperature control was achieved using a DF–101Z constant temperature magnetic stirrer (Shanghai Lichen Instrument Technology Co., Ltd., Shanghai, China), which was adjusted to various specified temperatures. The percentage removal at contact time t (R_t, %) of dye was calculated utilizing the following Equation (1):

$$R_t(\%) = \frac{A_0 - A_t}{A_0} \times 100 \quad (1)$$

where R_t (%) represented the removal rate of dye at time t, A_0 (mg/L) is the absorbance of the initial dye solution, and A_t (mg/L) is the absorbance of the dye solution at contact time t.

Unless otherwise specified, the adsorption experiments for kinetics, isotherms, thermodynamics, and dosage effects were conducted at the natural, unadjusted pH of the MB solution. This condition was chosen to establish a baseline performance of the BPs biosorbent under a scenario that minimizes pretreatment costs, thereby evaluating its practical applicability in a straightforward manner. The subsequent investigation on pH effect serves to mechanistically elucidate the role of electrostatic interactions and to explore the potential for further performance enhancement if pH adjustment is applicable.

2.5. Desorption and Reusability Experiments

The reusability of adsorbents was a crucial indicator for evaluating their performance and had been highly regarded in practical applications. To evaluate the reusability of biosorbents derived from BPs, the regeneration of spent BPs (specifically, MB-loaded BPs) was investigated using a 0.1 mol/L HCl aqueous solution. Briefly, following each adsorption experiment, the MB-loaded BPs were rinsed with purified water to remove any excess MB dye. Subsequently, they were immersed in 20 mL of 0.1 mol/L HCl aqueous solution and stirred for 5 min to facilitate the removal of adsorbed MB molecules on BPs. The regenerated BPs were then filtered and rinsed with purified water until the pH of the rinse water reached neutral levels before being reused in subsequent cycles of adsorption experiments.

2.6. Characterization

The phase composition and morphology of BPs were characterized by a X-ray Diffractometer (XRD, DX–2700, Dandong Haoyuan Instrument Co., Ltd., Dandong, China) and Scanning Electron Microscopy (SEM, SEM5000, CIQTEK Co., Ltd., Hefei, China). The functional group of BPs were examined by a Fourier Transform Infrared spectrometer (FTIR,

FTIR–7600, Tianjin Gangdong Sci. and Tech. Co., Ltd., Tianjin, China). N_2 adsorption-desorption isotherms were measured on a TriStar II Plus Version 3.03 (Micromeritics Instrument Corporation, Norcross, GA, USA), and the specific surface areas were determined using the Brunauer–Emmett–Teller method (S_{BET}).

3. Results and Discussion

3.1. Characterization of Raw and Alkali-Treated BPs

The structural and physicochemical properties of the raw BPs and those treated with 0.2 mol/L NaOH aqueous solution were characterized using XRD, FTIR spectroscopy, N_2 adsorption-desorption analysis, and SEM. The XRD patterns of both raw and alkali-treated BPs are presented in Figure 1a. Three distinct diffraction peaks at 2θ = 16.0°, 22.3°, and 34.8° were observed, corresponding to the (101), (002), and (004) crystal planes of Cellulose I, respectively [31]. After alkali treatment, the intensity and sharpness of the (002) peak increased significantly, and the (101) and (004) peaks became more pronounced and well-defined. This enhancement in crystallinity is attributed to the removal of amorphous components and soluble substances (e.g., polyphenols, soluble polysaccharides, and other small molecules) during the alkaline delignification process, which promotes intermolecular hydrogen bonding among cellulose hydroxyl groups and facilitates a more ordered arrangement of the molecular chains.

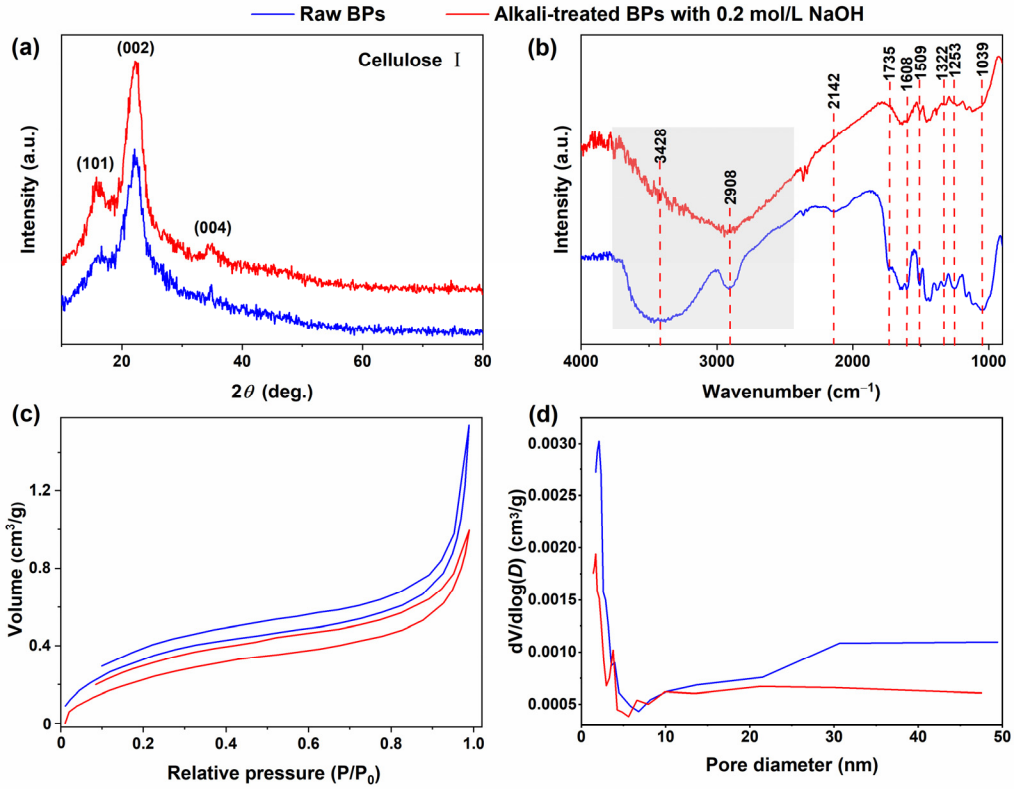


Figure 1. (**a**) XRD spectra, (**b**) FTIR spectra, (**c**) N_2 adsorption-desorption isotherms, and (**d**) Barrett–Joyner–Halenda pore size distribution curves of raw BPs and alkali-treated BPs with 0.2 mol/L NaOH aqueous solution.

The surface functional groups were investigated by FTIR spectroscopy within the range of 4000–900 cm^{-1} (Figure 1b). The spectrum of raw BPs exhibited a profile similar to other reported biomass adsorbents, with a broad and intense absorption band at 3428 cm^{-1} assigned to the O–H stretching vibration and a band at 2908 cm^{-1} corresponding to the asymmetric stretching of CH_2 groups [21–23,28]. In contrast, the spectrum of

alkali-treated BPs showed a merged and broadened absorption feature spanning from 3750 to 2450 cm^{-1}, encompassing both the O–H and CH_2 regions. This change indicates an effective alkali treatment, which likely increased the number of exposed surface hydroxyl groups and removed soluble small molecules, thereby enhancing the accessibility of cellulose's O–H and CH_2 groups. The absorption peaks in the regions of 1900–1500 cm^{-1} and 1500–1000 cm^{-1} are associated with various functional groups present in bamboo, including C=O stretching, aromatic ring skeleton vibrations, N–H bending, C–N stretching, C–H bending, C–O stretching, and $–[CH_2]_n–$ rocking vibrations [32]. These groups can be attributed to intrinsic bamboo components such as polyphenols, soluble polysaccharides, and other small molecules. Notably, the intensity of these characteristic peaks decreased or even disappeared after alkali treatment, further confirming the efficacy of the NaOH pretreatment in removing these soluble organic constituents.

The porous structure was evaluated using N_2 adsorption-desorption isotherms (Figure 1c). The isotherms for both samples can be classified as Type IV hysteresis loop, according to IUPAC classification, indicating the presence of disordered porous structures within the BPs [33]. The corresponding Barrett–Joyner–Halenda (BJH) pore size distribution curves are shown in Figure 1d. The textural parameters derived from the isotherms are summarized in Table 3. After alkali treatment, the S_{BET}, average pore diameter, and total pore volume all decreased compared to the raw BPs. This reduction corroborates the removal of amorphous or soluble components from the raw bamboo matrix, as suggested by the XRD and FTIR results.

The visual appearance and microstructure of the samples are shown in Figure 2. Macroscopically, the raw BPs exhibited a dull yellowish color (Figure 2a), whereas the alkali-treated BPs appeared as a brighter and cleaner yellow (Figure 2b), visually supporting the removal of organic chromophores by NaOH treatment. SEM images (Figure 2c,d) revealed a porous morphology for both samples, consistent with the results from the N_2 sorption experiments and confirming that the BPs possess a porous structure suitable for adsorption applications.

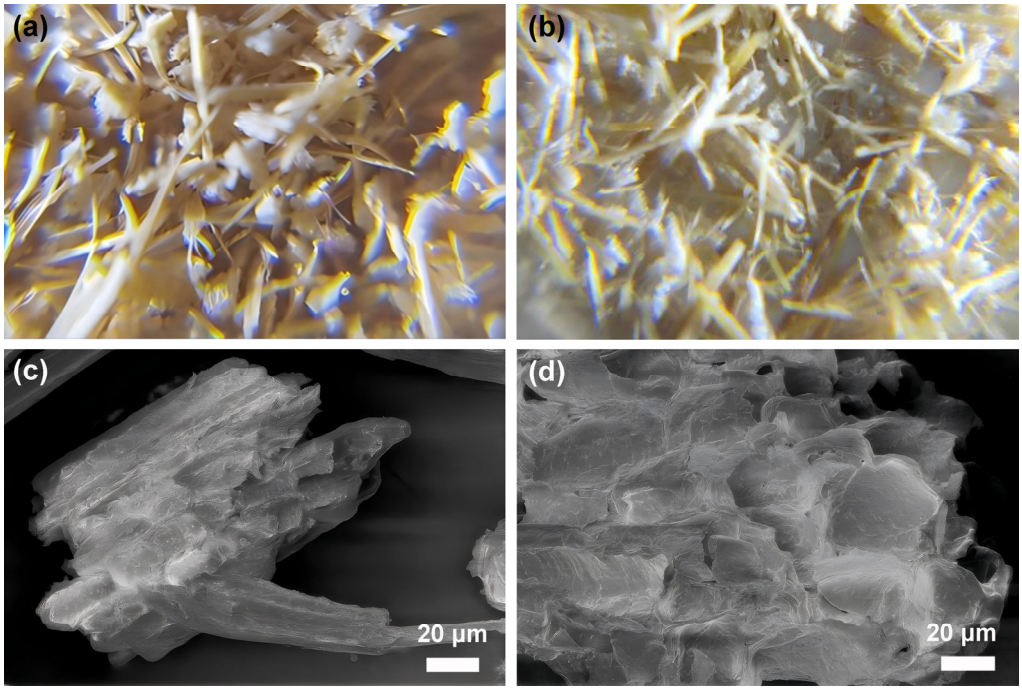


Figure 2. Macrophotograph of (**a**) raw BPs and (**b**) alkali-treated BPs with 0.2 mol/L NaOH aqueous solution; SEM images of (**c**) raw BPs and (**d**) alkali-treated BPs with 0.2 mol/L NaOH aqueous solution.

Table 3. Texture parameters of raw BPs and alkali-treated BPs with 0.2 mol/L NaOH aqueous solution.

Sample	S_{BET} (m^2/g)	Pore Diameter (nm)	Pore Volume (cm^3/g)
Raw BPs	1.34	6.06	0.002384
Alkali-treated BPs with 0.2 mol/L NaOH	1.05	4.35	0.001541

3.2. Enhanced Adsorption Kinetics and Preferential Adsorption for Cationic Dye Induced by Alkali Treatment

To elucidate the role of alkali treatment in enhancing performance and modifying surface charge properties, the adsorption of MB onto BPs was first systematically studied across a range of NaOH pretreatment concentrations (0.1–1.0 mol/L) under fixed conditions (20 mg/L dye, 10 g/L adsorbent, room temperature, no pH adjustment). The adsorption of the anionic dye AO7 was then evaluated under identical conditions as a contrasting probe to highlight the mechanism of electrostatic interaction.

The adsorption behavior of MB onto BPs pretreated with different NaOH concentrations is visually depicted in Figure 3. The biosorbent exhibited rapid and highly effective adsorption, with the NaOH concentration playing a crucial role. When the pretreatment concentration exceeded 0.2 mol/L, a notable lightening of the MB solution occurred within 10 min. Extending the contact time to 20 min resulted in visually colorless and transparent solutions for BPs treated with 0.2 to 1.0 mol/L NaOH. In contrast, BPs treated with 0.1 mol/L NaOH required 30 min to achieve a similar level of decoloration. These observations clearly indicate that NaOH concentration is a critical factor modulating the adsorption kinetics. It is hypothesized that higher alkali concentrations more effectively remove natural organic impurities (e.g., hemicellulose and lignin), thereby enhancing the surface negative charge and improving the accessibility of active sites, which favor faster electrostatic attraction with cationic MB [34]. Although the alkali pretreatment caused the release of colored organics, the subsequent thorough washing ensured their removal, which is corroborated by the clarity of all MB filtrates, even at the 40 min time point, as shown in Figure 3. Thus, interference from such leachates in evaluating the intrinsic adsorption performance is considered minimal.

The absorbance of the supernatant following MB adsorption by BPs at a concentration of 10.0 g/L, which were treated with NaOH solutions at varying concentrations (0.1–1.0 mol/L), was measured. The percentage removal R_t was calculated using Equation (1), and the results are illustrated in Figure 4a. Consistent with the visual observations in Figure 3, the quantitative data indicate a significant dependence of adsorption kinetics on the concentration of alkali pretreatment. For BPs treated with 0.1 mol/L NaOH, the MB removal rate was only 26.4% at 10 min. In contrast, BPs treated with 0.2, 0.4, and 0.6 mol/L NaOH achieved markedly higher removal rates of 62.5%, 63.5%, and 69.9%, respectively, at the same time interval. The performance was further enhanced with increasing alkali strength, as BPs treated with 0.8 and 1.0 mol/L NaOH exhibited removal rates of 78.0% and 87.7%, respectively. A contact time of 20 min proved to be a critical threshold. At this point, BPs treated with NaOH concentrations ranging from 0.2 to 1.0 mol/L all attained exceptional MB removal efficiencies exceeding 96.0%. The BPs treated with 0.1 mol/L NaOH, while slower, eventually reached a comparable removal rate of 96.5% at 30 min.

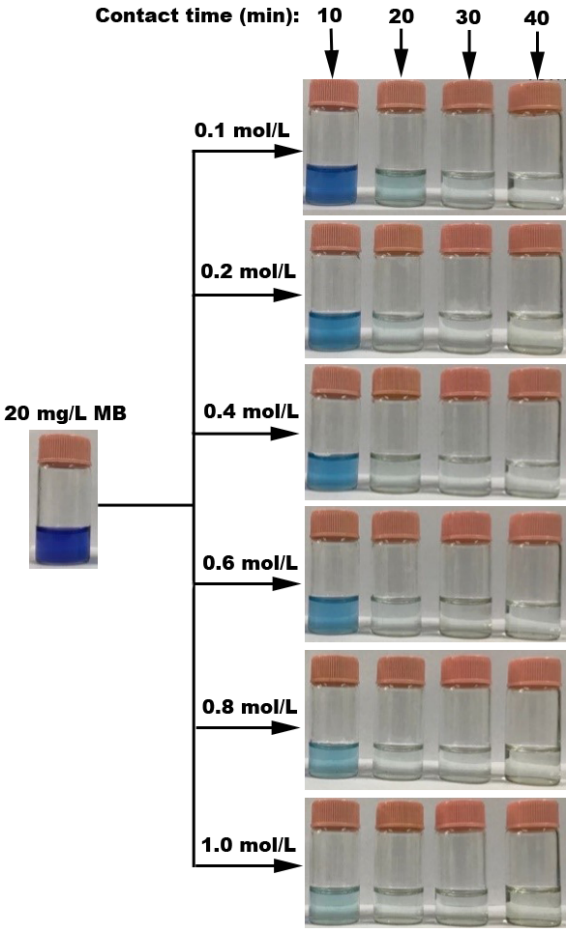


Figure 3. Photos of MB filtrate adsorbed by BPs biosorbent obtained by NaOH aqueous solution at varying concentrations (0.1–1.0 mol/L). ([BPs] = 1.0 g; [MB] = 20 mg/L; V = 100 mL; room temperature; pH without adjustment).

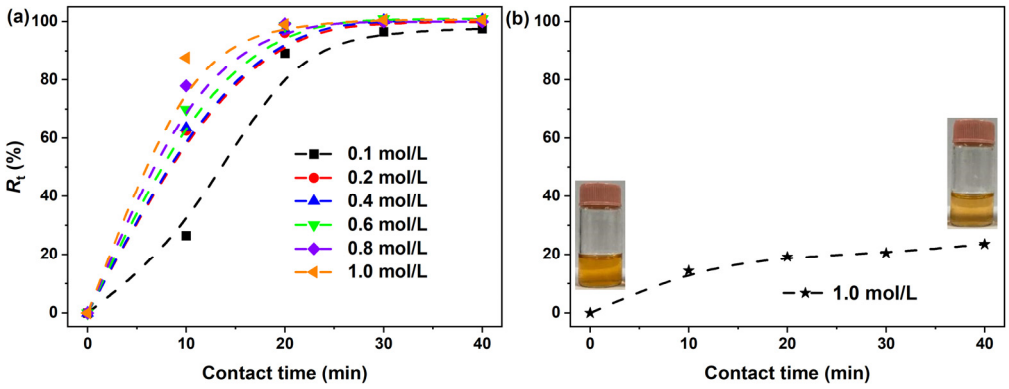


Figure 4. Impact of contact time on removal rate of (**a**) MB and (**b**) AO7 dyes onto BPs biosorbent obtained by NaOH aqueous solution at varying concentrations (0.1–1.0 mol/L). ([BPs] = 1.0 g; [MB/AO7] = 20 mg/L; V = 100 mL; room temperature; pH without adjustment).

To definitively attribute the high MB removal to the electrostatically driven mechanism rather than non-specific uptake, a parallel control experiment was conducted using the anionic dye AO7. As shown in Figure 4b, BPs (treated with 1.0 mol/L NaOH) exhibited a very limited affinity for AO7, achieving a removal rate of only 23.6% even after 40 min. This stark contrast definitively indicates that electrostatic interaction is the dominant adsorption mechanism. The markedly higher removal of MB compared to AO7 is attributed to the enhanced surface negative charge on BPs induced by the NaOH pretreatment, which

strongly favors electrostatic attraction with cationic dyes, This effectively transforms the biosorbent into a material with high affinity for cationic pollutants.

3.3. Effect of Dosage on MB Removal

Figure 5 shows the effect of adsorption of MB on BPs obtained by 0.2 mol/L NaOH aqueous solution at different dosages in 100 mL dye solution as a function of increase in the dosage of BPs. The data clearly indicates that adsorption increases with increase in the dosage quantity. The equilibrium adsorption capacity was estimated, and adsorption of MB is maximum (99.7%) when 1.0 g of BPs biosorbent is used.

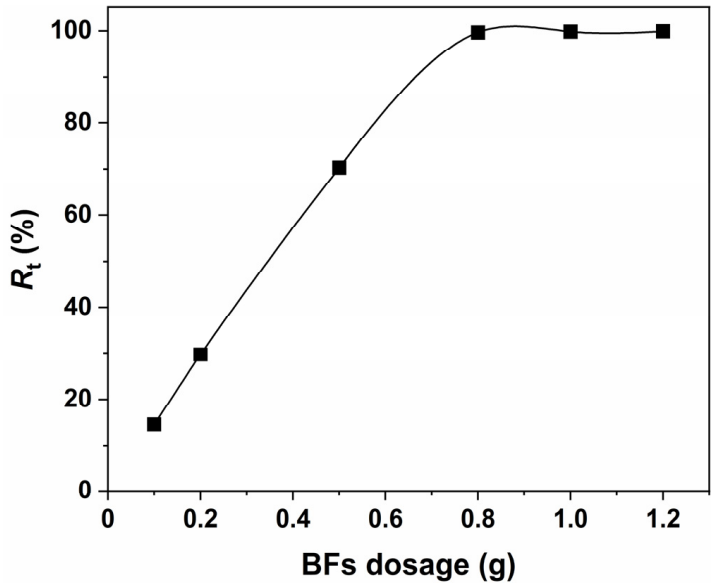


Figure 5. Effect of BPs dosage on MB removal. (BPs pre-treated with 0.2 mol/L NaOH; [MB] = 20 mg/L; V = 100 mL; t = 40 min; room temperature; pH without adjustment).

3.4. Effect of Temperature on MB Removal and Absorption Thermodynamics

The temperature had a strong effect on adsorption. Figure 6 showed the adsorption rate of BPs biosorbent synthesized with 0.2 mol/L NaOH aqueous solution at different temperatures. As observed, the adsorption rate of BPs biosorbent for MB dye decreased by elevating temperature from 303 K (30 °C) to 333 K (60 °C). Increasing the temperature was not conducive to the adsorption of MB dye onto BPs, which suggested an exothermic nature of the adsorption reaction. The Gibbs free energy change (ΔG^0, J/mol) at a set temperature could be evaluated using Equations (2)–(4), while the enthalpy change (ΔH^0, J/mol) and entropy change (ΔS^0, J/mol·K) could be obtained based on Van't Hoff Equation (Equation (5)) by the plot of log$K$ against $1/T$ (Figure 7). These thermodynamic parameters, including ΔG^0, ΔH^0 and ΔS^0 were calculated and summarized in Table 4.

$$q_e = \frac{V(C_0 - C_e)}{m} \quad (2)$$

$$\Delta G = -RT \ln K \quad (3)$$

$$K = \frac{q_e}{c_e} \quad (4)$$

$$\log K = -\frac{\Delta H}{2.303R} \times \frac{1}{T} + \frac{\Delta S}{2.303R} \quad (5)$$

where q_e (mg/g) represents the amount of MB dye adsorbed at adsorption-desorption equilibrium. C_0 (mg/L) and C_e (mg/L) denote the initial concentration of MB and the concentration of MB at adsorption-desorption equilibrium, respectively. Additionally, m (g)

refers to the mass of BPs, while V (mL) indicates the volume of the MB aqueous solution. The thermodynamic equilibrium constant, denoted as K (L/g), is determined at specific temperatures of 303, 308, 313, 318, 323, 328 and 333 K; it is defined as the ratio between q_e and C_e at these designated temperatures. Lastly, R (J/mol·K), representing the gas constant, has a value of 8.314.

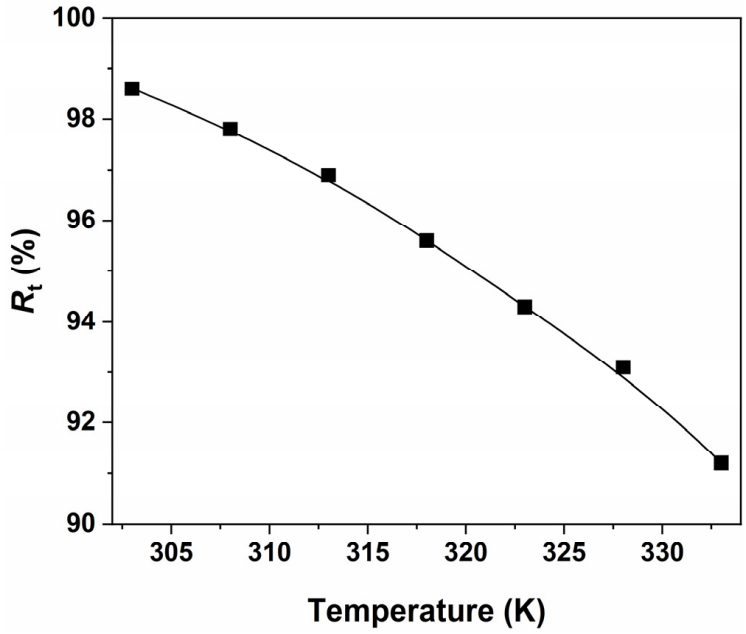


Figure 6. Impact of temperature on the removal of MB onto BPs biosorbent produced from biomass treating with 0.2 mol/L NaOH aqueous solution. ([BPs] = 1.0 g; [MB] = 20 mg/L; V = 100 mL; pH without adjustment; contact time = 40 min; temperature as indicated).

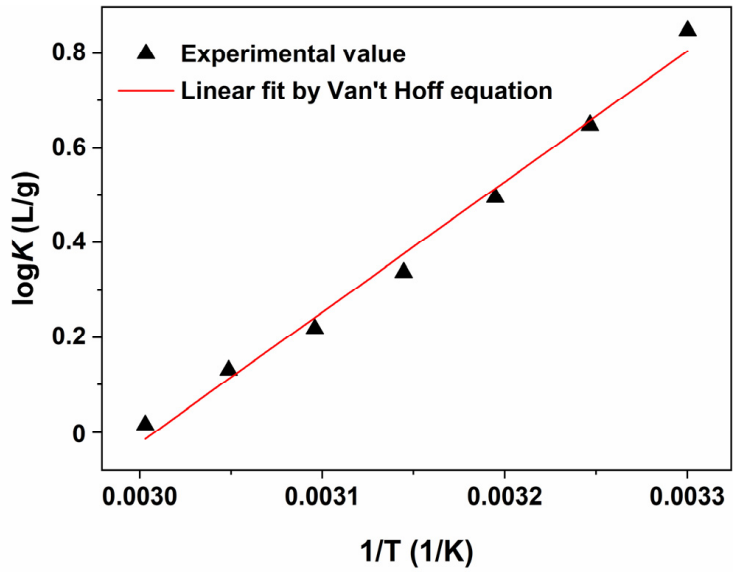


Figure 7. Van't Hoff plot fitting of MB removal data onto BPs biosorbent produced from biomass treating with 0.2 mol/L NaOH aqueous solution. ([BPs] = 1.0 g; [MB] = 20 mg/L; V = 100 mL; pH without adjustment; Contact time = 40 min; temperature as indicated).

Table 4. Thermodynamic parameters for the MB adsorption onto BPs produced by biomass treating with 0.2 mol/L NaOH aqueous solution.

Temperature (K)	Thermodynamic Parameters			R^2
	ΔG (J/mol)	ΔH (kJ/mol)	ΔS (J/mol·K)	
303	−4917.4			
308	−3820.3			
313	−2965.8			
318	−2051.6	−52.73	−158.6	0.9873
323	−1351.9			
328	−816.9			
333	−98.9			

The calculated thermodynamic parameters provide profound insight into the nature and mechanism of the MB adsorption process onto alkali-treated BPs. The consistently negative values of ΔG^0 (−4917.4 to −98.9 J/mol) confirm the spontaneity of the adsorption. Notably, the decrease in the magnitude of ΔG^0 with rising temperature aligns with the observed reduction in removal efficiency (Figure 6), indicating that the driving force for adsorption weakens at higher temperatures, a characteristic of an exothermic process.

This is directly supported by the large negative value of ΔH^0 (−52.73 kJ/mol), which unequivocally characterizes the adsorption as exothermic. The magnitude of ΔH^0 falls within the typical range for physicosorption mechanisms (−20 to −80 kJ/mol), strongly suggesting that the process is predominantly governed by interactions such as electrostatic attraction between the cationic MB and the negatively charged BPs surface [35]. The significant heat release points to substantial adsorbent–adsorbate affinity.

Furthermore, the negative value of ΔS^0 (−158.6 J/mol·K) reflects a decrease in randomness at the solid–solution interface. This is expected as mobile dye cations become more ordered upon fixation onto the adsorbent surface, with the loss of their translational freedom outweighing any entropic gain from solvent displacement. The high correlation coefficient (R^2 = 0.9873) of the Van't Hoff plot confirms the reliability of these thermodynamic interpretations. Collectively, the parameters ($\Delta G^0 < 0$, $\Delta H^0 < 0$, $\Delta S^0 < 0$) depict a spontaneous, exothermic adsorption process where enthalpy is the dominant driving force, resulting in a more ordered system, a profile that is consistent with monolayer coverage via strong surface interactions.

3.5. Effect of Initial MB Concentration and Adsorption Isotherms

The effects of MB initial concentration on adsorption with a contact time of 40 min in the range of 20–60 mg/L were shown in Figure 8; the BPs biosorbent used was one treated with 0.2 mol/L NaOH aqueous solution. As the initial concentration of MB aqueous solution increased from 20 mg/L to 60 mg/L, it was clear that the adsorption rate in Figure 8 decreased. It suggested that the adsorption was highly dependent on initial concentration of MB molecules. It was explained as follows. At the lower concentration, the ratio of the initial number of MB molecules to the available surface area of BPs adsorbent was low, and the fractional adsorption became independent of initial MB concentration. However, at the higher concentration, the available sites of adsorption became fewer, and hence the adsorption rate of BPs adsorbent was dependent upon initial MB concentration.

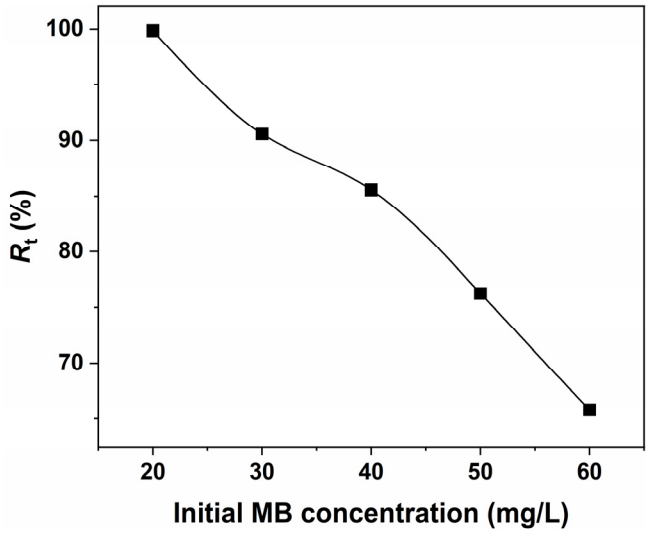


Figure 8. Influence of initial MB concentration on the removal capacity of BPs biosorbent produced from biomass treating with 0.2 mol/L NaOH aqueous solution. ([BPs] = 1.0 g; V = 100 mL; room temperature; pH without adjustment; contact time = 40 min; [MB] as indicated).

To investigate the adsorption mechanism between BPs and MB molecule, the experimental data were analyzed by Langmuir (Equation (6)) [36], Freundlich (Equation (7)) [37], Temkin (Equation (8)) [38], and Dubinin–Radushkevich (Equation (9)) [39] isotherm models, respectively.

$$\frac{C_e}{q_e} = \frac{1}{q_m} C_e + \frac{1}{K_L q_m} \quad (6)$$

$$\log q_e = \frac{1}{n} \log C_e + \log K_F \quad (7)$$

$$q_e = \frac{RT}{b_T} \ln K_T + \frac{RT}{b_T} \ln C_e \quad (8)$$

$$\ln q_e = \ln q_m - \beta \varepsilon^2 \ \left(E = \frac{1}{\sqrt{2\beta}}\right) \quad (9)$$

where q_e (mg/g) is the amount of MB adsorbed per unit mass of BPs at equilibrium, and q_m (mg/g) is the theoretical maximum monolayer adsorption capacity. C_e (mg/L) is the equilibrium concentration of MB in solution. The model-specific constants are defined as follows: K_L (L/mg) is the Langmuir constant related to the affinity of binding sites; K_F (mg/g) and n are the Freundlich constants indicative of adsorption capacity and intensity, respectively; K_T (L/mg) is the Temkin equilibrium binding constant; b_T (J/mol) is the Temkin constant related to the heat of adsorption; β (mol^2/J^2) is the Dubinin–Radushkevich constant, a parameter used to calculate the mean free energy of adsorption, E (kJ/mol); and ε (J/mol) is the Polanyi potential, calculated as $RT\ln(1 + 1/C_e)$. R represents the universal gas constant (8.314 J/mol·K), and T (K) is the absolute temperature at which the experiments were conducted.

Figure 9a–d showed Langmuir, Freundlich, Temkin, and Dubinin–Radushkevich models applied to the experimental data of the adsorption of MB dye onto BPs synthesized with 0.2 mol/L NaOH. The corresponding parameters calculated from these analyses are summarized in Table 5. Particular attention should be given to the calculated value of the squared correlation coefficient (R^2), which serve as an indicator of the goodness of fit. As observed in Table 5, the R^2 values obtained from the Langmuir, Freundlich, Temkin, and Dubinin–Radushkevich linear fits found to be 0.9947, 0.9025, 0.8426, and 0.6545, respectively. Notably, the Freundlich model intensity parameter n (2.79) exceeding

unity indicates a favorable adsorption process under the experimental conditions [37]. The highest correlation coefficient and the closest approach to unity for the Langmuir model strongly indicate that the adsorption of MB onto BPs is best described by the Langmuir isotherm. Similar monolayer adsorption behavior has also been observed in other porous material systems designed for enhanced VOC adsorption performance [40].

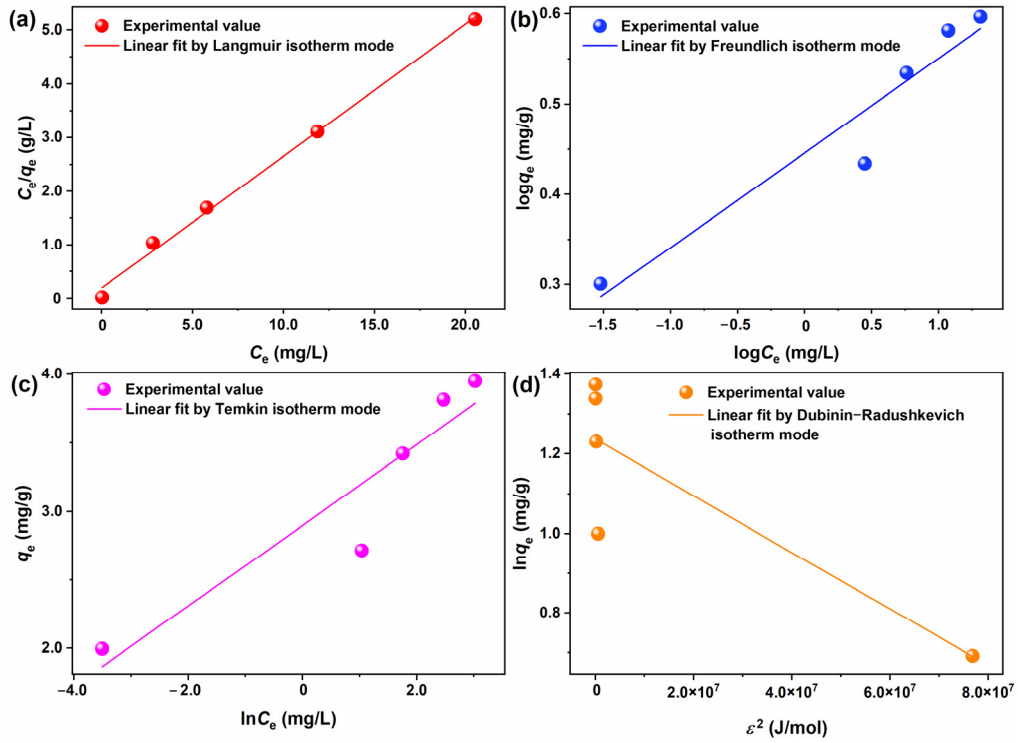


Figure 9. Linear fitting of MB adsorption isotherms onto BPs (pretreated with 0.2 mol/L NaOH) by (**a**) Langmuir, (**b**) Freundlich, (**c**) Temkin, and (**d**) Dubinin–Radushkevich isotherm models. ([BPs] = 1.0 g; V = 100 mL; room temperature; pH without adjustment; contact time = 40 min).

Table 5. Adsorption isotherms and related parameters for MB adsorption onto BPs pretreated with 0.2 mol/L NaOH.

Adsorption Isotherm	Langmuir			Freundlich			Temkin			Dubinin–Radushkevich			
Parameter	q_m (mg/g)	K_L (L/mg)	R^2	K_F (mg/g)	n	R^2	K_T (L/mg)	b_T (J/mol)	R^2	q_m (mg/g)	β (mol^2/J^2)	E (kJ/mol)	R^2
	4.1	1.35	0.9947	9.54	2.79	0.9025	1.00	8.42	0.8426	3.45	7.1×10^{-9}	8.39	0.6545

The results suggested that the adsorption of MB molecules onto BPs occurs in a monolayer fashion and takes place at specific, homogeneous sites on the surface of BPs. All adsorption sites are identical and exhibit the same adsorption energy; consequently, further adsorption does not take place once an adsorption site is occupied by an MB molecule. Furthermore, the BPs adsorbent demonstrates structural homogeneity, with negligible interactions between MB molecules adsorbed on adjacent sites. The saturation adsorption capacity of the BPs adsorbent was determined to be 4.1 mg/g via Langmuir linear fitting.

Although the Langmuir model provided the best fit, the complementary Temkin and Dubinin–Radushkevich models offer further mechanistic insights. The Temkin model, which accounts for adsorbent-adsorbate interactions, yielded a constant b_T of 8.42 J/mol, suggesting a moderate and uniform distribution of binding energies. Importantly, the mean free energy of adsorption (E) estimated from the Dubinin–Radushkevich model was 8.39 kJ/mol. This value lies near the characteristic boundary that is often used to

distinguish between physisorption ($E < 8$ kJ/mol) and chemisorption ($E > 16$ kJ/mol). The result indicates that the adsorption process is predominantly driven by physical forces, such as electrostatic attraction, but may involve specific interactions with an energy close to the transition range [39]. The comparatively lower R^2 values of the Temkin and Dubinin–Radushkevic models reinforce that the adsorption system is most accurately described by a homogeneous monolayer coverage (Langmuir model) rather than heterogeneous or pore-filling mechanisms.

3.6. Adsorption Kinetics

The studies on adsorption kinetics are essential for understanding the mechanism and rate-limiting steps of the adsorption process. To this end, the experimental data were analyzed using three widely recognized kinetic models: the pseudo-first-order (Equation (10)) [41], pseudo-second-order (Equation (11)) [42], and intraparticle diffusion (Equation (12)) [43] models.

$$\log(q_e - q_t) = -\frac{k_1}{2.303}t + \log q_e \tag{10}$$

$$\frac{t}{q_t} = \frac{1}{q_e}t + \frac{1}{k_2 q_e^2} \tag{11}$$

$$q_t = k_{id}t^{0.5} + C \tag{12}$$

where q_t and q_e (mg/g) are the adsorption capacities at time t and at equilibrium, respectively. k_1 (h^{-1}) and k_2 (g/mg·h) are the rate constants for the pseudo-first-order and pseudo-second-order models, respectively. For the intraparticle diffusion model (Weber–Morris model), K_{id} (mg/(g·$h^{0.5}$)) is the diffusion rate constant, and C (mg/g) is the intercept related to the boundary layer thickness.

The linear fittings of these models to the experimental data are presented in Figure 10, and the corresponding calculated parameters are summarized in Table 6. The correlation coefficient (R^2) is a key metric for evaluating the goodness of fit. As shown in Table 6, the pseudo-second-order model yielded the highest R^2 value (0.9666), significantly outperforming the pseudo-first-order model (R^2 = 0.5161). This indicates that the adsorption kinetics of MB onto BPs are best described by the pseudo-second-order model, suggesting that the rate-limiting step may involve chemisorption-like interactions, such as electron sharing or exchange between the adsorbent and adsorbate [44].

To further elucidate the mass transfer mechanism, the intraparticle diffusion model was applied. The plot of q_t versus $t^{0.5}$ (Figure 10c) shows a multi-linear trend, implying that the adsorption process occurs in multiple stages. The first, steeper region can be attributed to the instantaneous surface adsorption or boundary layer diffusion, while the second, more gradual linear region represents the intra-particle diffusion stage. The calculated intra-particle diffusion rate constant k_{id} is 1.8073 mg/(g·$h^{0.5}$). Critically, the fitted line does not pass through the origin (C = 0.6581 mg/g $\neq$ 0), which clearly demonstrates that intra-particle diffusion is involved but is not the sole rate-controlling step [43]. The adsorption process is therefore governed by a combination of boundary layer diffusion and intra-particle diffusion. This finding is consistent with the porous structure of the alkali-treated BPs, which facilitates both rapid initial surface binding and subsequent slower diffusion into the pore network.

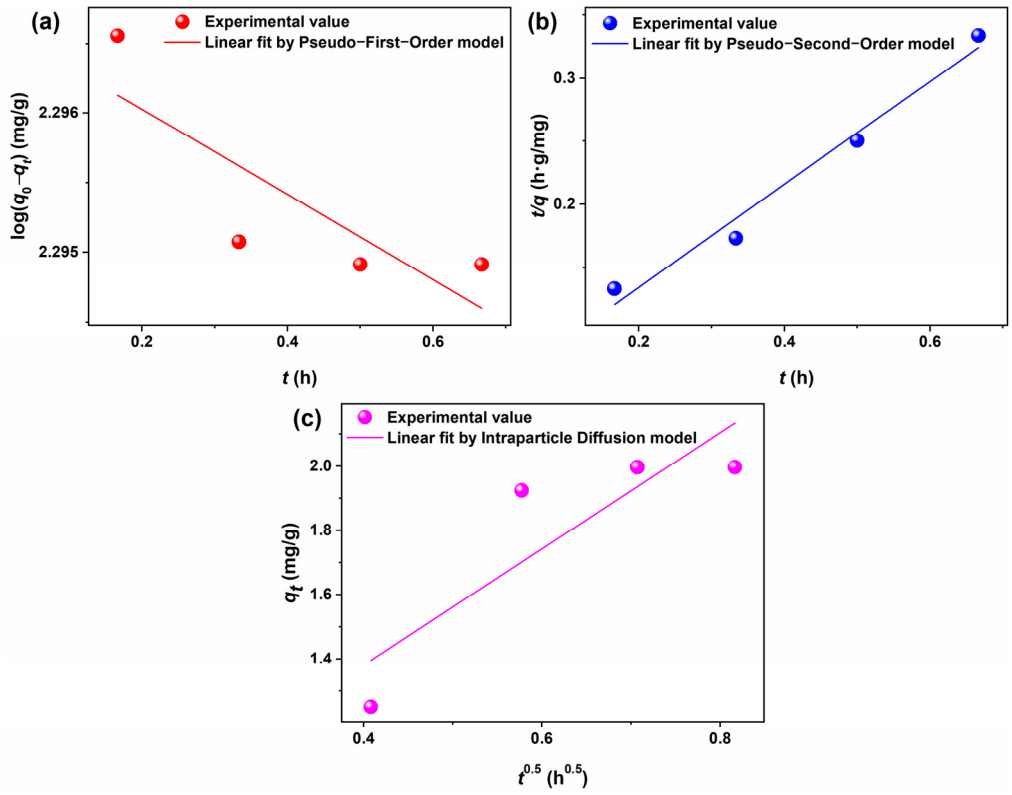


Figure 10. Linear fitting of MB adsorption kinetics onto BPs (pretreated with 0.2 mol/L NaOH) by (**a**) pseudo-first-order, (**b**) pseudo-second-order, and (**c**) intraparticle diffusion kinetic models. ([BPs] = 1.0 g; [MB] = 20 mg/L; V = 100 mL; room temperature; pH without adjustment).

Table 6. Kinetic models and related parameters for adsorption of MB dye onto BPs pretreated with 0.2 mol/L NaOH at room temperature.

Kinetic Model	Pseudo-First-Order			Pseudo-Second-Order			Intraparticle Diffusion		
Parameter	q_e (mg/g)	K_1 (h^{-1})	R^2	q_e (mg/g)	K_2 (g/mg·h)	R^2	K_{id} (mg/g·$h^{0.5}$)	C (mg/g)	R^2
	198.0	0.0070	0.5156	2.4567	3.1261	0.9666	1.8073	0.6581	0.6461

3.7. Effect of Solution pH

While the preceding sections evaluated the adsorption performance under the natural pH of the dye solution, simulating a low-cost operational mode. To gain deeper mechanistic insight into the adsorption process, the influence of solution pH was investigated. For lignocellulosic materials like alkali-treated bamboo, the surface charge density is highly pH-dependent. At higher pH, the deprotonation of surface functional groups (e.g., –COOH, –OH) increases the net negative charge on the adsorbent, which would enhance electrostatic attraction with cationic dyes.

The adsorption experiments were performed in the pH range from 5 to 9 for an initial MB concentration of 60 mg/L with 1.0 g BPs, and the results were provided in Figure 11. As observed, the MB adsorption onto BPs improved as the solution pH increased. The removal efficiency exhibited a remarkable enhancement, escalating from 28.7% at pH = 5 to 84.9% at pH = 9. This trend is consistent with the expected surface charge behavior. This increased adsorption at alkaline pH can be attributed to the enhanced electrostatic attraction between the negatively charged surface of BPs and the positively charged MB cations. Conversely, at lower pH, the adsorbent surface becomes more positively charged due to protonation, leading to electrostatic repulsion with MB cations and competition with

excess H^+ ions for adsorption sites, resulting in lower removal efficiency. These findings strongly support the proposed electrostatic interaction as a dominant mechanism in the adsorption process.

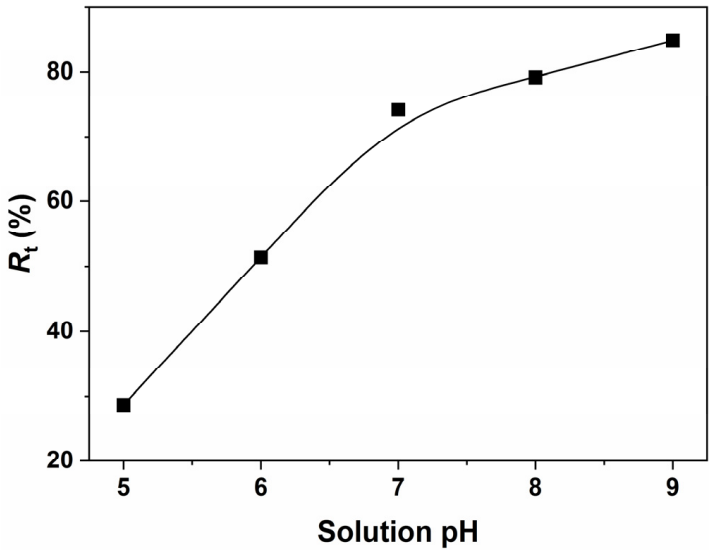


Figure 11. Impact of solution pH on MB removal onto BPs biosorbent produced from biomass treating with 0.2 mol/L NaOH aqueous solution. ([BPs] = 1.0 g; [MB] = 60 mg/L; *V* = 100 mL; room temperature; contact time = 40 min).

3.8. Regeneration

The reusability of materials had been highly valued in the practical application, and it was an important indicator to evaluate the performance of materials, because it would greatly reduce the cost of using similar materials, and the adsorbents were no exception. To estimate the reusable efficacy of BPs adsorbent, the regeneration of the spent BPs adsorbent was studied using 0.1 mol/L HCl aqueous solution. Figure 12 showed the performance of BPs adsorbent synthesized with 0.2 mol/L NaOH aqueous solution within eight cycles of regeneration study. From Figure 12, it could be concluded that washing with 0.1 mol/L HCl aqueous solution could regenerate the adsorption capacity of BPs for MB dye. The adsorption rate observed for the recycled BPs adsorbent was 91.2% even after eight successive cycles, suggesting that the BPs composite was a potential adsorbent with good stability. The performance losses might be attributed to the blockage of some active sites on BPs surface, the changes in chemistry or structure as well as the mass loss of BPs adsorbent. Therefore, the regeneration aspect of the BPs confirmed its cost-effectiveness, which was of utmost importance in the industrial application as the adsorbent could be recycled for multiple uses [45].

3.9. Overall Performance Assessment and Comparative Perspective

The overall performance of the alkali-pretreated bamboo powder (BPs) biosorbent is evaluated by integrating key findings from this study. The q_{max} for MB, as determined by the Langmuir model, is 4.1 mg/g (Section 3.4). This value represents a baseline performance achieved under natural, unadjusted pH conditions, chosen to reflect a low-cost operational scenario. Notably, as shown in Section 3.7 (Figure 11), the adsorption capacity exhibits significant enhancement potential under alkaline conditions, where stronger electrostatic attraction prevails.

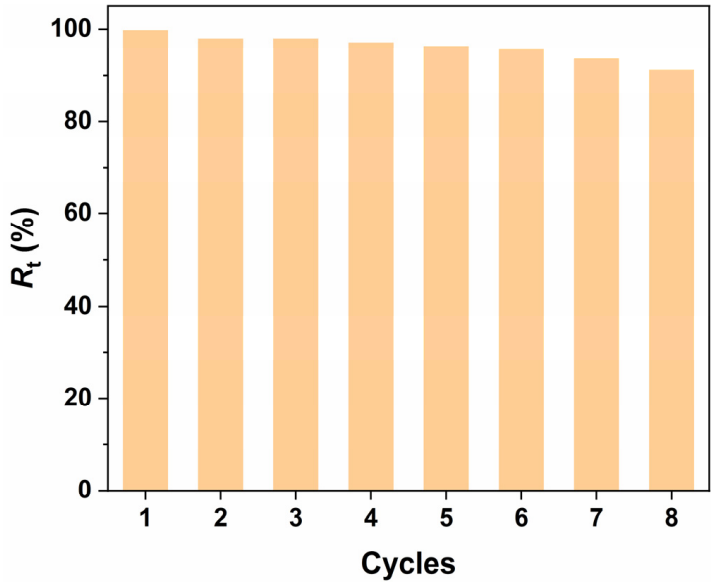


Figure 12. Effect of BPs regeneration times on the MB removal rate ([BPs] = 1.0 g; [MB] = 20 mg/L; V = 100 mL; room temperature; pH without adjustment; contact time = 40 min).

When compared quantitatively to the q_{max} values of other biomass-derived adsorbents for dyes (Table 1), the capacity of the present BPs is moderate. However, a holistic assessment reveals that this system delivers a distinctive and synergistic combination of attributes: exceptionally rapid adsorption kinetics (over 96% removal within 20 min), a high affinity for cationic dyes driven by electrostatic interaction, and excellent regenerability with stable performance over multiple cycles. Critically, these functionalities are achieved through a simple, room-temperature alkali pretreatment, foregoing the energy-intensive carbonization or complex chemical modifications typically required for high-capacity adsorbents. Therefore, this work highlights a balanced performance profile that prioritizes process efficiency, targeted removal, sustainability, and cost-effectiveness alongside capacity, presenting a compelling practical strategy for cationic dye wastewater treatment.

4. Conclusions

A highly efficient biosorbent derived from bamboo powders (BPs) was successfully synthesized through a simple and mild alkali pretreatment. Systematic investigations confirmed that NaOH pretreatment concentration ($\geq$0.2 mol/L) played a decisive role in enhancing the adsorption performance. The optimized BPs exhibited exceptionally rapid adsorption kinetics, achieving over 96% removal of cationic MB within 20 min. The adsorption process was best described by the Langmuir isotherm model, indicating monolayer adsorption on homogeneous sites, with a maximum capacity of 4.1 mg/g, and followed pseudo-second-order kinetics. Thermodynamic analysis revealed the process to be spontaneous and exothermic. Importantly, the alkali-treated BPs demonstrated a strong affinity for cationic dyes, effectively removing MB (96.5%), while showing much lower removal for anionic AO7 (23.6%), a behavior attributed to the enhanced surface negative charge induced by the pretreatment, leading to strong electrostatic attraction with cationic dyes. The biosorbent also exhibited outstanding stability and reusability, maintaining a removal efficiency above 91.2% after eight consecutive adsorption-desorption cycles using dilute HCl as eluent. In summary, this study shows that a straightforward alkali pretreatment can unlock the potential of bamboo biomass, yielding a biosorbent that combines rapid kinetics, high efficiency for cationic dyes via electrostatic attraction, and

remarkable regenerability. This approach offers a cost-effective, environmentally friendly, and practical strategy for the targeted treatment of cationic dye-contaminated wastewater.

Author Contributions: Conceptualization, Y.X. and Q.W.; validation, J.Y., R.X., Z.J. and Y.Z.; investigation, Q.W., Y.X., J.Y., R.X., Z.J. and Y.Z.; resources, Y.X., Q.W. and F.X.; data curation, Q.W., Y.X., J.Y., R.X., Z.J. and Y.Z.; writing—original draft, Q.W. and Y.X.; writing—review and editing, Y.X. and F.X.; supervision, Y.X. and F.X.; project administration, Y.X. and F.X.; funding acquisition, Y.X. and F.X. All authors have read and agreed to the published version of the manuscript.

Funding: This work was financially supported by the Innovative Experimental Project of Higher Education Institutions in Sichuan Province, China; College Student Innovation and Entrepreneurship Training Program, China (202510649019, S202510649127, 2025XJ060).

Data Availability Statement: Data are contained within the article.

Conflicts of Interest: The authors declare no conflicts of interest.

References

1. Negi, A. Natural dyes and pigments: Sustainable applications and future scope. *Sustain. Chem.* **2025**, *6*, 23. [CrossRef]
2. Yuan, J.; Yang, H.; Huang, W.; Liu, S.; Zhang, H.; Zhang, X.; Peng, X. Design strategies and applications of cyanine dyes in phototherapy. *Chem. Soc. Rev.* **2025**, *54*, 341–366. [CrossRef]
3. Kayani, K.F.; Mohammed, S.J.; Mustafa, M.S.; Aziz, S.B. Dyes and their toxicity: Removal from wastewater using carbon dots/metal oxides as hybrid materials: A review. *Mater. Adv.* **2025**, *6*, 5391–5409. [CrossRef]
4. Swaminaathan, P.; Thamarai, P.; Yaashikaa, P.R.; Saravanan, A.; Vickram, A.S. Microbial bioremediation of dyes, metals, and microplastics for ecological sustainability. *Energy Ecol. Environ.* **2025**, *10*, 45–65. [CrossRef]
5. Upadhyay, R.; Przystaś, W.; Dave, B. Myco-remediation of synthetic dyes: A comprehensive review on contaminant alleviation mechanism, kinetic study and toxicity analysis. *Int. J. Environ. Sci. Technol.* **2025**, *22*, 521–538. [CrossRef]
6. Parida, S.; Mandal, A.K.; Behera, A.K.; Patra, S.; Nayak, R.; Behera, C.; Jena, M. A comprehensive review on phycoremediation of azo dye to combat industrial wastewater pollution. *J. Water Process Eng.* **2025**, *70*, 107088. [CrossRef]
7. Lianmawii, L.; Singh, K.B.; Singh, N.R.; Singh, N.M. A review: Photocatalytic degradation of dyes by metal sulfide nanoparticles. *Braz. J. Chem. Eng.* **2025**, *42*, 1–30. [CrossRef]
8. Ayub, A.; Wani, A.K.; Chopra, C.; Sharma, D.K.; Amin, O.; Wani, A.W.; Singh, A.; Manzoor, S.; Singh, R. Advancing Dye Degradation: Integrating Microbial Metabolism, Photocatalysis, and Nanotechnology for Eco-Friendly Solutions. *Bacteria* **2025**, *4*, 15. [CrossRef]
9. Ahmaruzzaman, M.; Roy, S.; Singha, A.; Rtimi, S.; Aminabhavi, T.M. Emerging nanotechnologies in adsorption of dyes: A comprehensive review of carbon and metal oxide-based nanomaterials. *Adsorption* **2025**, *31*, 34. [CrossRef]
10. Un Nisa, F.; Naseem, K.; Aziz, A.; Hassan, W.; Fatima, N.; Najeeb, J.; Ur Rehman, S.; Khalid, A.; Khan, M.E. Comparative analysis of dye degradation methods: Unveiling the most effective and environmentally sustainable approaches, a critical review. *Rev. Inorg. Chem.* **2025**, *45*, 275–306. [CrossRef]
11. Khan, W.A.; Varanusupakul, P.; Haq, H.U.; Arain, M.B.; Boczkaj, G. Applications of nanosorbents in dispersive solid phase extraction/microextraction approaches for monitoring of synthetic dyes in various types of samples: A review. *Microchem. J.* **2025**, *208*, 112419. [CrossRef]
12. Khan, A.; Khan, S.A.; Sajid, M.; Shukla, S.; Manchanda, A.; Khan, T.A.; Chaudhry, S.A. Multifunctional hydrogel adsorbents for wastewater remediation: Current trends and future directions. *J. Mol. Liq.* **2025**, *435*, 128129. [CrossRef]
13. Georgin, J.; Ramos, C.G.; de Oliveira, J.S.; Dehmani, Y.; El Messaoudi, N.; Meili, L.; Franco, D.S. A critical review of the advances and current status of the application of adsorption in the remediation of micropollutants and dyes through the use of emerging bio-based nanocomposites. *Sustainability* **2025**, *17*, 2012. [CrossRef]
14. Kassa, A.; Engida, A.; Endaye, M. Eco-friendly adsorbents for industrial dye removal: A comprehensive review of low-cost alternatives. *Desalin. Water Treat.* **2025**, *323*, 101362. [CrossRef]
15. Wang, N.; Zhang, R.; Liu, K.; Zhang, Y.; Shi, X.; Sand, W.; Hou, B. Application of nanomaterials in antifouling: A review. *Nano Mater. Sci.* **2024**, *6*, 672–700. [CrossRef]
16. Cano, F.J.; Reyes-Vallejo, O.; Sánchez-Albores, R.M.; Sebastian, P.J.; Cruz-Salomón, A.; Hernández-Cruz, M.d.C.; Montejo-López, W.; González Reyes, M.; Serrano Ramirez, R.d.P.; Torres-Ventura, H.H. Activated Biochar from Pineapple Crown Biomass: A High-Efficiency Adsorbent for Organic Dye Removal. *Sustainability* **2025**, *17*, 99. [CrossRef]

17. Mohamed, M.M. Acid dye removal: Comparison of surfactant-modified mesoporous FSM-16 with activated carbon derived from rice husk. *J. Colloid Interface Sci.* **2004**, *272*, 28–34. [CrossRef]
18. Saad, S.A.; Isa, K.M.; Bahari, R. Chemically modified sugarcane bagasse as a potentially low-cost biosorbent for dye removal. *Desalination* **2010**, *264*, 123–128. [CrossRef]
19. Namasivayam, C.; Muniasamy, N.; Gayatri, K.; Rani, M.; Ranganathan, K. Removal of dyes from aqueous solutions by cellulosic waste orange peel. *Bioresour. Technol.* **1996**, *57*, 37–43. [CrossRef]
20. Khattri, S.D.; Singh, M.K. Colour removal from dye wastewater using sugar cane dust as an adsorbent. *Adsorpt. Sci. Technol.* **1999**, *17*, 269–282. [CrossRef]
21. Cardoso, N.F.; Lima, E.C.; Pinto, I.S.; Amavisca, C.V.; Royer, B.; Pinto, R.B.; Alencar, W.S.; Pereira, S.F. Application of cupuassu shell as biosorbent for the removal of textile dyes from aqueous solution. *J. Environ. Manag.* **2011**, *92*, 1237–1247. [CrossRef] [PubMed]
22. Marungrueng, K.; Pavasant, P. High performance biosorbent (*Caulerpa lentillifera*) for basic dye removal. *Bioresour. Technol.* **2007**, *98*, 1567–1572. [CrossRef]
23. Mahmoodi, N.M.; Arami, M.; Bahrami, H.; Khorramfar, S. Novel biosorbent (Canola hull): Surface characterization and dye removal ability at different cationic dye concentrations. *Desalination* **2010**, *264*, 134–142. [CrossRef]
24. Saha, P. Assessment on the removal of methylene blue dye using tamarind fruit shell as biosorbent. *Water Air Soil Pollut.* **2010**, *213*, 287–299. [CrossRef]
25. Alencar, W.S.; Acayanka, E.; Lima, E.C.; Royer, B.; de Souza, F.E.; Lameira, J.; Alves, C.N. Application of Mangifera indica (mango) seeds as a biosorbent for removal of Victazol Orange 3R dye from aqueous solution and study of the biosorption mechanism. *Chem. Eng. J.* **2012**, *209*, 577–588. [CrossRef]
26. Ansari, R.; Seyghali, B.; Mohammad-khah, A.; Zanjanchi, M.A. Application of Nano Surfactant Modified Biosorbent as an Efficient Adsorbent for Dye Removal. *Sep. Sci. Technol.* **2012**, *47*, 1802–1812. [CrossRef]
27. Gong, R.; Ding, Y.; Li, M.; Yang, C.; Liu, H.; Sun, Y. Utilization of powdered peanut hull as biosorbent for removal of anionic dyes from aqueous solution. *Dye. Pigment.* **2005**, *64*, 187–192. [CrossRef]
28. Kankılıç, G.B.; Metin, A.Ü.; Tüzün, İ. Phragmites australis: An alternative biosorbent for basic dye removal. *Ecol. Eng.* **2016**, *86*, 85–94. [CrossRef]
29. Alencar, W.S.; Lima, E.C.; Royer, B.; dos Santos, B.D.; Calvete, T.; da Silva, E.A.; Alves, C.N. Application of aqai stalks as biosorbents for the removal of the dye Procion Blue MX-R from aqueous solution. *Sep. Sci. Technol.* **2012**, *47*, 513–526. [CrossRef]
30. Romão, A.L.E.; de Oliveira Damasceno, R.I.; Alves, C.R.; Carrilho, E.N.V.M. Nanomodified bamboo (*Phyllostachys aurea*) biomass: Its adsorbent features in the removal of dyes from water under high salinity conditions. *Environ. Sci. Pollut. Res.* **2025**, *32*, 22004–22020. [CrossRef]
31. Singh, A.; Ranawat, B.; Meena, R. Extraction and characterization of cellulose from halophytes: Next generation source of cellulose fibre. *SN Appl. Sci.* **2019**, *1*, 1311. [CrossRef]
32. Meng, L.Z.; He, Y.B. *Organic Spectroscopic Analysis*, 1st ed.; Wuhan University Press: Wuhan, China, 1997; pp. 26–35.
33. Thommes, M.; Kaneko, K.; Neimark, A.V.; Olivier, J.P.; Rodriguez-Reinoso, F.; Rouquerol, J.; Sing, K.S.W. Physisorption of gases, with special reference to the evaluation of surface area and pore size distribution (IUPAC Technical Report). *Pure Appl. Chem.* **2015**, *87*, 1051–1069. [CrossRef]
34. Yu, Y.; Liu, Z.; Chen, X.; Liu, S.; Duan, C.; Xi, H. Water-based synthesis of nanoscale hierarchical metal-organic frameworks: Boosting adsorption and catalytic performance. *Nano Mater. Sci.* **2023**, *5*, 361–368. [CrossRef]
35. Foo, K.Y.; Hameed, B.H. Insights into the modeling of adsorption isotherm systems. *Chem. Eng. J.* **2010**, *156*, 2–10. [CrossRef]
36. Langmuir, I. The constitution and fundamental properties of solids and liquids. *J. Am. Chem. Soc.* **1917**, *39*, 1848–1906. [CrossRef]
37. Freundlich, H. Über die Adsorption in Lösungen. *J. Phys. Chem.* **1907**, *57*, 385–470. [CrossRef]
38. Tempkin, M.I.; Pyzhev, V. Kinetics of ammonia synthesis on promoted iron catalyst. *Acta Phys. Chim. Sin.* **1940**, *12*, 327–356.
39. Dubinin, M.M. The potential theory of adsorption of gases and vapors for adsorbents with energetically nonuniform surfaces. *Chem. Rev.* **1960**, *60*, 235–241. [CrossRef]
40. Liang, K.; Guo, W.; Li, L.; Cai, H.; Zhang, H.; Li, J.; Xu, F.; Yan, J.; Lv, D.; Xi, H. Defect-induced synthesis of nanoscale hierarchically porous metal-organic frameworks with tunable porosity for enhanced volatile organic compound adsorption. *Nano Mater. Sci.* **2024**, *6*, 467–474. [CrossRef]
41. Lagergren, S. Zur theorie der sogenannten adsorption geloster stoffe, Kungliga Svenska Vetenskapsakademiens. *Handlingar* **1898**, *24*, 1–39.
42. Ho, Y.S.; McKay, G. Pseudo-second order model for sorption processes. *Process Biochem.* **1999**, *34*, 451–465. [CrossRef]
43. Weber, W.J., Jr.; Morris, J.C. Kinetics of adsorption on carbon from solution. *J. Sanit. Eng. Div.* **1963**, *89*, 31–59. [CrossRef]

44. Aadil, M.; Khan, M.A.; Repycha, S.A.; Kaseem, M. Utilizing a defective MgO layer for engineering multifunctional Co-MOF hybrid materials with tailored leaf-like and polyhedral structures for optimal electrochemical and photocatalytic activities. *Nano Mater. Sci.* **2024**, *6*, 548–564. [CrossRef]
45. Rianjanu, A.; Marpaung, K.D.P.; Melati, E.K.A.; Aflaha, R.; Wibowo, Y.; Mahendra, I.P.; Yulianto, N.; Widakdo, J.; Triyana, K.; Wasisto, H.S.; et al. Integrated adsorption and photocatalytic removal of methylene blue dye from aqueous solution by hierarchical Nb_2O_5@PAN/PVDF/ANO composite nanofibers. *Nano Mater. Sci.* **2024**, *6*, 96–105. [CrossRef]

Disclaimer/Publisher's Note: The statements, opinions and data contained in all publications are solely those of the individual author(s) and contributor(s) and not of MDPI and/or the editor(s). MDPI and/or the editor(s) disclaim responsibility for any injury to people or property resulting from any ideas, methods, instructions or products referred to in the content.